Experimental Characterization and Computer Vision-Assisted Detection of Pitting Corrosion on Stainless Steel Structural Members

RILEY J. MUEHLER, JOHUA B. VENZ, MICHAEL D. TODD and LONG WANG

ABSTRACT

Pitting corrosion is a prevalent form of corrosive damage that can weaken, damage, and initiate failure in corrosion-resistant metallic materials. For instance, 304 stainless steel is commonly utilized in various structures (e.g., miter gates, heat exchangers, and storage tanks), but is prone to failure through pitting corrosion and stress corrosion cracking under mechanical loading, regardless of its high corrosion resistance. The pit growth typically follows a sigmoidal trend with an initial high growth rate during nucleation, followed by an eventual saturation limit, which will ultimately lead to material failure. In this study, to better understand the pitting corrosion damage development, controlled corrosion experiments were conducted to generate pits on 304 stainless steel specimens with and without mechanical loading. The pit development over time was characterized using a high-resolution laser scanner. In addition, to achieve scalable and automatic assessment of pitting corrosion conditions, a convolutional neural network-based computer vision algorithm was adopted and implemented to identify the existence of pitting damage.

INTRODUCTION

Pitting corrosion is a form of localized corrosion that most commonly occurs in marine environment due to the presence of chloride ions (Cl^-) in salt spray, which can affect various structures, including miter gates, ships, docks, bridges, and nuclear plants [1]. While stainless steel is inherently resistant against general corrosion through alloying of Chromium and Nickel, pitting corrosion can bypass the passivating oxide layer on stainless steel with the presence of permeable ions or cracks in the oxide layer, leading to local anodic behavior in the metal underneath the protective layer. When exposed to an electrolytic solution (e.g., one with high Cl^- concentration), local galvanic cells will be formed and cause the growth of pits. Corrosive products can often cover damage around local cathodic regions, making damage difficult to detect [2].

Riley J. Muehler, Joshua B. Venz, and Long Wang*, California Polytechnic State University, San Luis Obispo, CA, 93407, USA.
Michael D. Todd, University of California-San Diego, La Jolla, CA, 92093, USA.
*Corresponding author e-mail: lwang38@calpoly.edu

Pitting corrosion can not only compromise the mechanical properties of structural steels, but also cause intergranular stress corrosion cracks (SCCs), augmenting material fracture mode [3]. It remains very challenging to isolate, measure, or reliably characterize the SCCs, due to their complex propagation at micro-scale. In addition, although load-bearing structural members may exhibit different corrosion behavior depending on the loading conditions, to the best of the authors' knowledge, limited studies have been conducted on the effect of mechanical loading on the propagation of pitting corrosion.

Furthermore, in the context of pitting corrosion detection and evaluation, current techniques are relatively limited and ineffective. For instance, the "Standard Guide for Examination and Evaluation of Pitting Corrosion" (i.e., ASTM G46-21) outlines several different ways to evaluate pitting corrosion, including visual inspection, profilometry, metal penetration, statistical modelling, and eddy currents [4]. Another commonly used approach is the field signature method [5]. These techniques typically require highly trained human inspectors, have inconsistent measurements, and are non-versatile for different structures. On the other hand, with the recent advancements in machine learning and artificial intelligence, computer vision technique has been demonstrated promising for detecting structural anomalies (e.g., concrete cracks, rebar exposure, general corrosion, and dynamic modes) [6-8].

Therefore, this study aims to not only better understand the pitting corrosion damage development through controlled experiments, but also develop computer vision algorithms to detect pitting corrosion in an automatic, efficient, and scalable manner. In particular, a series of accelerated pitting corrosion experiments was designed and performed on 304 stainless steel specimens with and without mechanical loading. The pit morphologies were characterized using a high-resolution laser scanner. In addition, convolutional neural networks (CNNs) were adopted and implemented to detect the existence of pitting damage based on images of steel specimens.

EXPERIMENTAL DETAILS

Accelerated Pitting Corrosion Experiment

Here, AISI 304 stainless steel (50.8 × 63.5 × 4.7625 mm^3, Metals Depot) was used as the test subject, which was corroded in an iron (III) chloride ($FeCl_3$, Sigma-Aldrich) aqueous solution. To be specific, the $FeCl_3$ solution was prepared by dissolving 16.22 g of $FeCl_3$ powders in 200 mL of deionized (DI) water through stirring. The solution was then heated to and maintained at about 50 °C using a hotplate. Prior to being submerged in the corrosive solution, each steel specimen was carefully sanded to remove the surficial protective oxide layers and washed with DI water. Steel specimens subjected to different corrosion time periods (e.g., 1, 2, and 3 hr in this study) could be readily generated in a consistent manner, so that pit development at different time instants could be investigated. Once the desired corrosion timeframe was reached, the specimen was removed from the corrosive solution, washed thoroughly with DI water, and air dried for at least a day before inspection.

Microstructural analysis of the pit damage was performed using scanning electron microscopy (SEM) imaging. In addition, to characterize the pit morphology in detail, all corroded specimens were inspected using a Micro-Vu Vertex 312UC system that

was equipped with an LSM4-2 laser distance scanner. A central region of 25.4 × 25.4 mm^2 on each specimen was inspected using the LSM4-2 laser to obtain representative statistical features of pit morphology. The resolutions of the laser scan along vertical and horizontal directions were 4 microns and about 0.03 microns, respectively.

Mechanical Load-Coupled Corrosion Experiment

This study aims to address the current knowledge gap of the effects of mechanical loading conditions on pitting corrosion development through conducting controlled multiphysics experiments. Figure 1 shows the schematics of the load-coupled corrosion experimental setup designed in this study. To be specific, each AISI 304 stainless steel specimen (50.8 × 342.9 × 4.7625 mm^3, Metals Depot) was fully submerged in the $FeCl_3$ aqueous solution, which was maintained at about 50 °C using heaters. Note that the corrosive solution and specimens were prepared following the same procedures described in the previous section. In addition, to apply mechanical loading on the specimens in a consistent and controllable manner, a four-point bending setup was designed, where the deadweight could be readily changed to achieve desired stress levels in the specimens (e.g., 28 MPa maximum tensile and compressive stresses in this study). Similar to the accelerated corrosion experiments, once the desired corrosion timeframe was reached, each specimen was washed thoroughly with DI water and air dried before being inspected using the laser scanner.

COMPUTER VISION-BASED DAMAGE DETECTION FRAMEWORK

This study also adopted and implemented the computer vision technique to more efficiently identify the existence of pitting damage. Figure 2 demonstrates the workflow established in this study for training and implementing the CNN algorithm for detection of pitting corrosion. First, the CNN was trained by establishing an image library. Based on the experimental samples obtained from the accelerated corrosion tests, the training and testing image library was established by partitioning seven high-resolution (443-by-340 pixel) images to sub-images of 31-by-31-pixel. The partitioning was necessary for generating a library large enough to test the efficacy of the CNN from limited numbers of specimens. These partitioned images were then manually labeled into two identification classes (i.e., pits and no pits). The training library has a total of 1,093

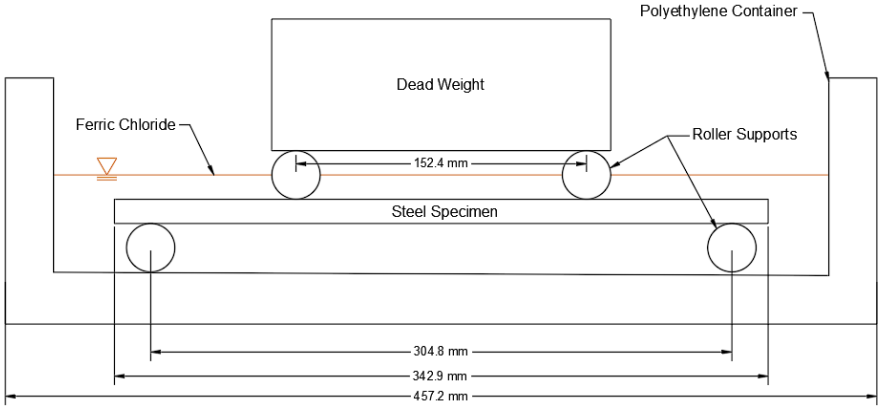

Figure 1. Schematics of mechanical load-coupled corrosion experimental setup.

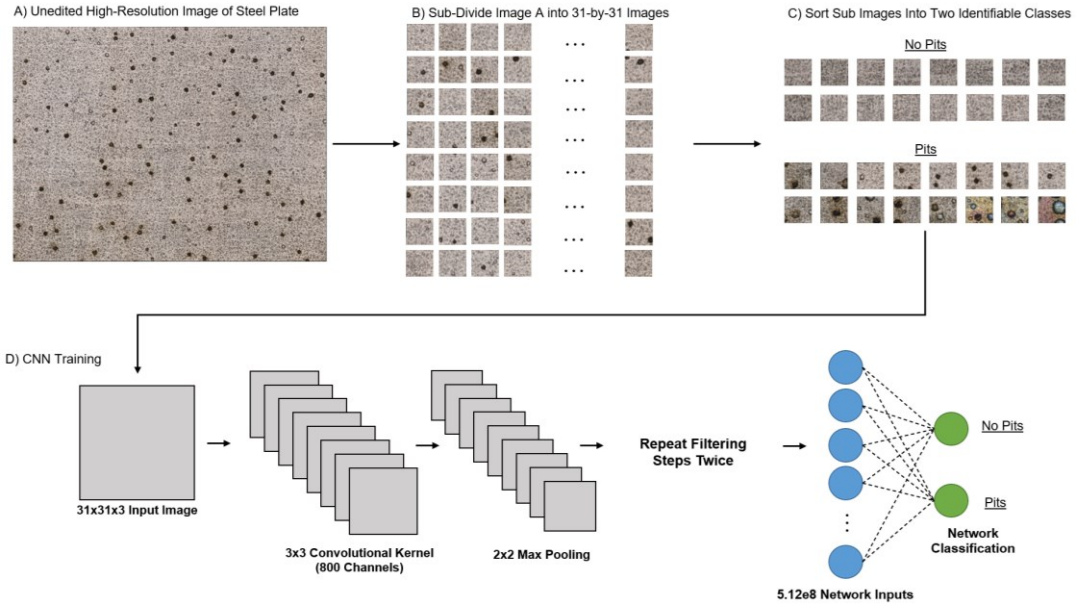

Figure 2. Schematics of the workflow of CNN-based computer vision technique for identifying the existence of pitting damage.

images with 740 images containing pits and 353 images without pits. After the classes were established, the library was then imported into the CNN algorithm in the MATLAB software, where it was separated further into a training set (70 %) and a validation set (30%) for each class.

The algorithm also performed image augmentations to prevent the CNN from memorizing the training set, forcing it to search for image features instead. These augmentation procedures involved randomly reflecting the images as well as translating the image up to 30 pixels horizontally and vertically. The MATLAB-based CNN algorithm then used the training and validation sets to train and test the CNN, respectively. The CNN trainer included three 3×3 kernel convolutional layers separated by three 2×2 max pooling layers with associated rectified linear unit (ReLU) layers, as shown in Figure 2. The results of these filters were then passed into the fully connected layer, connecting every input node to every output node by multiplying the input by a weight matrix and then adding a bias vector. This allowed the CNN algorithm to interpret the results of the training data and input images to create the neural network. It should be noted that to implement the CNN technique in the field, the same algorithm could be used by expanding the library with images of structures in the field and laboratory specimens, so that the trained CNN algorithm could inform the inspectors whether pit damage is present and the severity of the pitting.

RESULTS AND DISCUSSION

Pitting Corrosion Experiments

First, the accelerated pitting corrosion experimental procedures optimized in this study were found capable of exclusively generating pit damage on stainless steel, which facilitated the investigation of pit development under different conditions. Figure 3

shows the SEM images of a specimen subjected to a three-hour accelerated corrosion experiment. One can observe that the pits possessed diameters ranging from 1 micron to several millimeters. This indicates that pitting was a corrosive process that began at micro-scale and propagated to macro-scale through an autocatalytic reaction. The pits were found randomly distributed with distinguishable local anodic and cathodic regions. In addition, from the high magnification images (Figures 3c and 3d), intergranular cracks were also observed, which are typically the result of preferable corrosion at chromium-depleted zones adjacent to the austenitic grain boundaries of the stainless steel.

In addition, this study also utilized a high-resolution laser scanner to characterize the morphologies of pits on each corroded specimen. The laser scan data, composed of three-dimensional (3D) coordinates, were calibrated for each specimen's surface slope, so that the baseline depth (i.e., without pits) was 0 and pit depth was negative value along z direction. Table I summarizes pit inspection results of both the accelerated corrosion and the load-coupled corrosion experiments. It can be seen that pit depths were highly consistent among different specimens with low standard deviations and exhibited a steady increase in tandem with corrosion time periods (i.e., 1 hr to 3 hr). The pit depths were also relatively similar among all three load cases (i.e., no loading, tension, and compression).

On the other hand, pit surface opening areas were found affected by the mechanical loading conditions. In particular, compared to the average surface opening area of pits on the specimens subjected only to corrosion (without loading), tensile stress significantly decreased the pit opening areas, whereas compressive stress increased the areas. The difference in surface opening area became more prominent when comparing the depth-to-area ratios of the pits, which clearly showed that pits on the tension side of specimens had significantly higher ratios. Note that the calculated average surface opening areas exhibited relatively high standard deviations, which could be caused by pits developed at different stages that were all captured by the laser scanner.

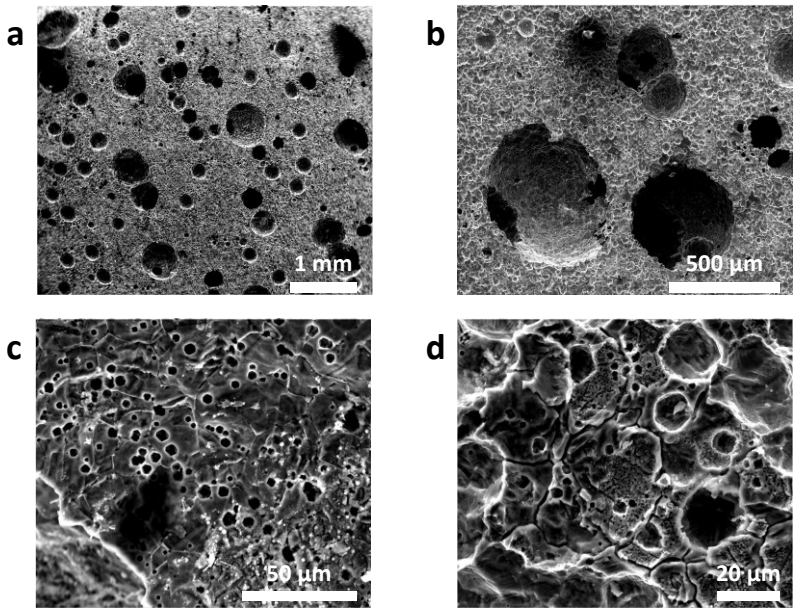

Figure 3. SEM images under different magnifications of pits on a stainless steel specimen subjected to a three-hour accelerated corrosion experiment.

TABLE I. EXPERIMENTAL RESULTS OF THE 50 DEEPEST PITS

Sample			Top 50 Deepest Pits				
Time (hr)	**Load Case**	**Load Type**	**Average Depth (mm)**	**Standard Deviation (mm)**	**Average Surface Opening Area (mm^2)**	**Standard Deviation (mm^2)**	**Depth/Area Ratios of the 50 Deepest Pits**
1	Corrosion Only	N/A	-0.221	0.0364	0.0331	0.0082	6.68
	28 MPa	Compression	-0.284	0.0077	0.0362	0.0137	7.86
		Tension	-0.266	0.0134	0.0081	0.0061	32.86
2	Corrosion Only	N/A	-0.327	0.0351	0.0300	0.0213	10.91
	28 MPa	Compression	-0.344	0.0335	0.1338	0.0978	2.57
		Tension	-0.324	0.0322	0.0085	0.0065	38.14
3	Corrosion Only	N/A	-0.454	0.0275	0.0277	0.0236	16.41
	28 MPa	Compression	-0.412	0.0485	0.0617	0.0447	6.68
		Tension	-0.377	0.0670	0.0176	0.0161	21.43

To further demonstrate the difference in pit morphologies caused by mechanical loading, Figure 4 shows color contour plots of the tension and compression sides of a specimen subjected to a three-hour load-coupled corrosion experiment. Although both tension and compression sides had similar numbers of pits (297 and 183 pits, respectively), the pits on the compression side (Figure 4b) were very visible due to their large surface opening areas. Figures 4c-4f show zoomed-in views of the morphologies of representative individual pits, which demonstrate that pits generated under tensile stress were as deep, but more localized.

Due to the observed pit morphologies, under the same stress level, pits developed under tensile stress could induce higher stress concentration effects and initiate earlier SCC and material failures. In addition, since the surface opening area of pits generated under compressive stress was larger, visual inspectors and computer vision-based techniques could identify those pits more easily. On the other hand, pits under tension may be challenging to be visually detected due to their small surface areas, even though they could be more likely to initiate failures in structural steels.

Computer Vision-Based Damage Identification

This study also trained and implemented a CNN algorithm for detecting pitting damage based on images of steel specimens. After being trained using the limited image library outlined previously, the CNN algorithm had an identification accuracy of nearly 84.4%. Here, the accuracy was used as a measure of how often the CNN was correct overall in identifying both true positive (i.e., pits exist) and true negative (i.e., no pit exists) classifications. The accuracy of trained CNN was considered relatively high, given the limited dataset and low resolution of the sub-images due to the level of partitioning. Figure 5a shows an example of the CNN output for the validation images, where both classification results were correct. In addition, to avoid overfitting to the training data, six epochs were used for training in this study. As shown in Figure 5b, the sixth epoch

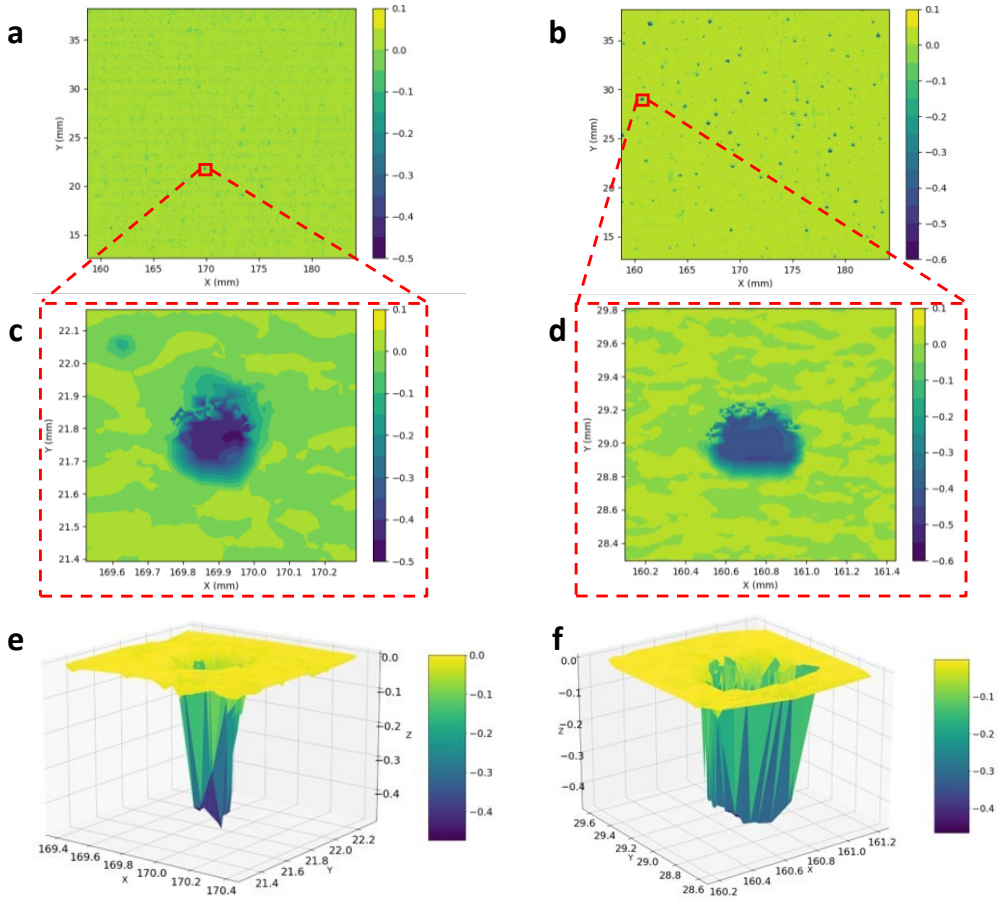

Figure 4. Color contour plots of 25.4 × 25.4 mm^2 central regions on the a) tension and b) compression sides of a steel specimen subjected to 3-hr of load-coupled corrosion experiment. c) and d) Zoomed-in views of individual pits highlighted in a) and b), respectively. e) and f) Visualization of 3D morphologies of pits shown in c) and d), respectively.

training began approaching to 100% accuracy. This indicates that further training using the current dataset would likely lead to overfitting to this specific training library, instead of learning the features of pitting corrosion. The CNN algorithm could be further trained with a larger image library that includes images of both laboratory specimens and structures in the field, which would allow the algorithm to learn more image features, achieve higher accuracy, and ultimately become sufficiently robust to

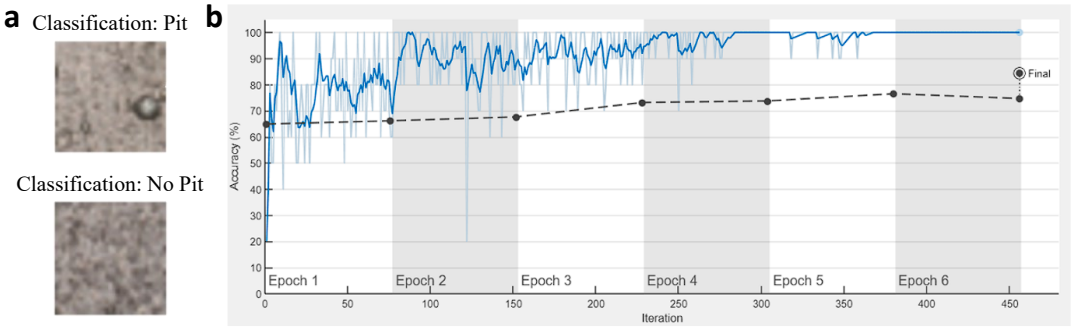

Figure 5. a) Examples of validation outputs of the trained CNN algorithm. b) Accuracy plot during training with blue line showing the smoothed training data and black line showing the validation accuracy at the end of each iteration.

detect pitting damage in the field. Furthermore, computer vision-enabled inspection can potentially be coupled with computational corrosion models to predict pit development and its effects on structural performance, which will significantly facilitate timely structural maintenance.

CONCLUSION

This study aims to not only develop experimental procedures to consistently generate pitting corrosion on structural steels, including accelerated corrosion experiments and load-coupled corrosion experiments, but also train and implement the CNN-based computer vision technique for detecting pitting damage. The developed corrosion experimental procedures were highly controllable and can be potentially implemented to study complex corrosion behavior of various metals. The laser scan-based results indicated that applied load could affect the pit morphology, where compressive stress led to larger surface opening area, whereas tensile stress induced much smaller openings. Therefore, pits formed under tensile stress could increase stress concentration more significantly, leading to earlier SCC and material failures. Furthermore, the CNN algorithm trained in this study possessed a high accuracy of 84.4%, even with the limited library currently available, making it a promising tool for detecting pitting corrosion in an efficient, automatic, and scalable manner.

ACKNOWLEDGEMENT

This research is supported by the United States Army Corps of Engineers. The authors also acknowledge the help from undergraduate research assistants at Cal Poly, including Nathan Kessenich, Savannah Wood, Nicholas Mackechnie, Maddie Necochea, and Christopher Chau.

REFERENCES

1. Van Wijk, Lorenzo, et al. “Corrosion-related Accidents in Petroleum Refineries: Lessons Learned from Accidents in EU and OECD Countries.” *European Union*, 2013.
2. Caines, Susan, et al. “Analysis of Pitting Corrosion on Steel under Insulation in Marine Environments.” *Journal of Loss Prevention in the Process Industries*, vol. 26, 2013, pp. 1466–1483.
3. Kolkman, H. J., et al. “Aircraft Crash Caused by Stress Corrosion Cracking.” *Journal of Engineering for Gas Turbines and Power*, vol. 118, no. 1, 1996, pp. 146–149.
4. ASTM Standard G46-21, 2021, “Standard Guide for Examination and Evaluation of Pitting Corrosion.” *ASTM International*, West Conshohocken, PA, 2021.
5. Gan, Fangji, et al. “Investigation of Pitting Corrosion Monitoring Using Field Signature Method.” *Measurement*, vol. 82, 2016, pp.46-54.
6. Matthaiou, Achilleas. “Corrosion Detection with Computer Vision and Deep Learning.” *Developments in the Analysis and Design of Marine Structures*, 2021, pp. 289-296.
7. Huang, Xinyuan, et al. “Surface Damage Detection for Steel Wire Ropes Using Deep Learning and Computer Vision Techniques.” *Measurement*, vol. 161, 2020, p. 107843.
8. Santos, R., et al. “Detection of Exposed Steel Rebars Based on Deep-Learning Techniques and Unmanned Aerial Vehicles.” *Automation in Construction*, vol. 139, 2022, p. 104324.